EXTENSIONS OF MULTIVARIATE COEFFICIENT OF VARIATION CONTROL CHARTS

HEBA NASR AWWAD AYYOUB

UNIVERSITI SAINS MALAYSIA

2021

EXTENSIONS OF MULTIVARIATE COEFFICIENT OF VARIATION CONTROL CHARTS

by

HEBA NASR AWWAD AYYOUB

Thesis submitted in fulfilment of the requirements for the degree of Doctor of Philosophy

February 2021

ACKNOWLEDGEMENT

I wish to express my honor and gratefulness to Allah for His inspiration and blessings during my Ph.D. study. Without His Will, this thesis will never be completed successfully.

I also would like to take this opportunity to express my deepest appreciation and thanks to my supervisor, Professor Michael Khoo Boon Chong from the School of Mathematical Sciences, Universiti Sains Malaysia, for his consistent guidance, suggestions, advice, and great efforts in helping me from the beginning of my study until the end. His professional expertise, insight, and knowledge of Statistical Quality Control have greatly benefited me. I have acquired valuable knowledge and research skills from him throughout my Ph.D. study.

I also would like to extend my profound gratitude to the School of Mathematical Sciences, Universiti Sains Malaysia, for the generous provision of facilities and space, such as the postgraduate student's lab and computer lab. I was able to conduct my research in a conducive environment. My special thanks also goes to the library of Universiti Sains Malaysia for its full range of useful reading materials, especially reference books and latest journals that are required in the completion of my Ph.D. study.

My deepest thanks are extended to my beloved parents, Mr. Nasr Ayyoub and Mrs. Chanhom Srikudkao. Without their support, tolerance, and encouragement, this thesis could not have come to fruition. To my brothers and sisters: Sami, Fares, Maha, Sana, and Nada, thanks for all the love and support. To my husband, Abdullah Al-Jawarneh, thank you so much for your motivation and encouragement. To my son and daughter, Shadi and Selena, thanks for being in my life. I am grateful to my beloved family members for always standing by my side through thick and thin.

I would also like to express my sincere gratitude to all my friends in the School of Mathematical Sciences, Universiti Sains Malaysia. To those who have indirectly contributed to my study, your kindness means a lot to me. Thank you very much.

Finally, being a housewife, mother and student, especially amid COVID-19 and homesickness, is challenging, but I did it. Alhamdulillah, I am proud of myself. All these memories are unforgettable.

Heba N. Ayyoub

TABLE OF CONTENTS

ACKNOWLEDGEMENT .... **ii**

TABLE OF CONTENTS .... **iv**

LIST OF TABLES .... **vii**

LIST OF FIGURES .... **xii**

LIST OF ABBREVIATIONS .... **xiv**

LIST OF NOTATIONS .... **xvi**

LIST OF APPENDICES .... **xix**

ABSTRAK ……. .... **xx**

ABSTRACT… .... **xxii**

CHAPTER 1 INTRODUCTION **1**

1.1 Statistical Process Control 1

1.2 Problem Statement 3

1.3 Objectives of the Study 5

1.4 Significance of the Study 5

1.5 Limitations of the Study 6

1.6 Organization of the Thesis 7

CHAPTER 2 A REVIEW OF RELATED CHARTS AND THEIR PERFORMANCE MEASURES **9**

2.1 Introduction 9

2.2 Literature Review of the Univariate and Multivariate CV Charts 10

2.2.1 An overview of CV charts 10

2.2.2 An overview of MCV charts 12

2.3 An Overview of Existing Univariate and Multivariate Charts with Measurement Errors 16

2.4 Basic Definitions and Assumptions of the Sample MCV 18

2.5 Performance Measures of the MCV Charts 22

2.5.1 Performance measures of the Shewhart-MCV chart...................... 22

2.5.2 Performance measures of the EWMA-γ^2 chart 24

2.6 Linearly Covariate Error Model 34

2.7 Summary 36

CHAPTER 3 PROPOSED UPPER-SIDED VSI EWMA CHART FOR MONITORING THE MCV 37

3.1 Introduction 37

3.2 Adaptive Charts.. 38

3.3 Upper-sided VSI EWMA-γ^2 Chart... 40

3.4 Performance Measures and Optimization Algorithm of the Upper-sided VSI EWMA-γ^2 Chart 42

3.5 Numerical Analyses of the Upper-sided VSI EWMA-γ^2 Chart 45

3.6 Performance Comparisons of the Upper-sided VSI EWMA-γ^2 Chart with Existing Upper-sided MCV Charts 51

3.7 An Illustrative Example 55

3.8 Summary 58

CHAPTER 4 PROPOSED SHEWHART-MCV CHARTS WITH MEASUREMNET ERRORS 59

4.1 Introduction 59

4.2 Two One-sided Shewhart-MCV Charts with Measurement Errors 60

4.3 Effects of a False Assumption of No Measurement Error on the Two One-sided Shewhart-MCV Charts 64

4.4 Numerical Analyses of the Two One-sided Shewhart-MCV Charts with Measurment Errors 66

4.5 An Illustrative Example 83

4.6 Summary 91

CHAPTER 5 EFFECTS OF THE PRESENCE OF MEASUREMENT ERRORS ON THE SHEWHART AND EWMA MCV CHARTS 92

5.1 Introduction 92

5.2 Shewhart-MCV Chart with a Linearly Covariate Error Model 93

5.3 Upper-sided Shewhart-MCV Chart in the Presence of Measurement Errors 97

5.3.1 Performance measures of the upper-sided Shewhart-MCV chart with measurement errors 98

5.3.2 Numerical analyses of the upper-sided Shewhart-MCV chart with measurement errors 100

5.4 Upper-sided EWMA-γ^2 Chart in the Presence of Measurement Errors 110

5.4.1 Performance measures of the upper-sided EWMA-γ^2 chart with measurement errors 110

5.4.2 Numerical analyses of the upper-sided EWMA-γ^2 chart with measurement errors 112

5.5 An Illustrative Example 124

5.6 Summary 127

CHAPTER 6 CONCLUSION 128

6.1 Introduction 128

6.2 Contributions and Findings in the Thesis 129

6.3 Suggestions for Future Research 131

REFERENCES 133

APPENDICES

LIST OF PUBLICATIONS

LIST OF TABLES

Page

Table 2.1 Strengths and weaknesses of the Shewhart-MCV and EWMA-γ^2 charts 33

Table 3.1 Past studies on adaptive charts 39

Table 3.2 Optimal parameters (λ^*, h_2^*, W^*, K^*) in minimizing the ATS_1 value and the corresponding (ATS_1, $SDTS_1$) values of the upper-sided VSI EWMA-γ^2 chart for h_1 = 0.1, p = 2, $n \in$ {7, 10, 15, 20}, $\gamma_0 \in$ {0.1, 0.3, 0.5} and $\tau \in$ {1.1, 1.25, 1.5, 2.0} 47

Table 3.3 Optimal parameters (λ^*, h_2^*, W^*, K^*) in minimizing the ATS_1 value and the corresponding (ATS_1, $SDTS_1$) values of the upper-sided VSI EWMA-γ^2 chart for h_1 = 0.1, p = 3, $n \in$ {7, 10, 15, 20}, $\gamma_0 \in$ {0.1, 0.3, 0.5} and $\tau \in$ {1.1, 1.25, 1.5, 2.0} 48

Table 3.4 Optimal parameters (λ^*, h_2^*, W^*, K^*) in minimizing the ATS_1 value and the corresponding (ATS_1, $SDTS_1$) values of the upper-sided VSI EWMA-γ^2 chart for h_1 = 0.1, p = 4, $n \in$ {7, 10, 15, 20}, $\gamma_0 \in$ {0.1, 0.3, 0.5} and $\tau \in$ {1.1, 1.25, 1.5, 2.0} 49

Table 3.5 Optimal parameters (λ^*, h_2^*, W^*, K^*) in minimizing the ATS_1 value and the corresponding (ATS_1, $SDTS_1$) values of the upper-sided VSI EWMA-γ^2 chart for h_1 = 0.1, p = 5, $n \in$ {7, 10, 15, 20}, $\gamma_0 \in$ {0.1, 0.3, 0.5} and $\tau \in$ {1.1, 1.25, 1.5, 2.0} 50

Table 3.6 Optimal parameters (λ^*, h_2^*, W^*, K^*) and the corresponding $EATS_1$ values of the upper-sided VSI EWMA-γ^2 chart for h_1 = 0.1, $p \in$ {2, 3, 4, 5}, $n \in$ {7, 10, 15, 20}, $\gamma_0 \in$ {0.1, 0.3, 0.5} and (τ_{min}, τ_{max}) = (1, 2) 51

Table 3.7 (ATS_1, $SDTS_1$) values for the upper-sided Shewhart-MCV, VP MCV, EWMA-γ^2 and VSI EWMA-γ^2 charts, for h_1 = 0.1, $p \in$ {2, 3, 4, 5}, $n \in$ {7, 10, 15, 20}, γ_0 = 0.1 and $\tau \in$ {1.1, 1.25, 1.5, 2.0} .. 53

Table 3.8 EATS$_1$ values for the upper-sided Shewhart-MCV, VP MCV, EWMA-γ^2 and VSI EWMA-γ^2 charts, for h_1 = 0.1, $p \in \{2, 3, 4, 5\}$, $n \in \{7, 10, 15, 20\}$, $\gamma_0 \in \{0.1, 0.3, 0.5\}$ and (τ_{min}, τ_{max}) = (1, 2) 54

Table 3.9 A comparison among the VSI EWMA-γ^2 chart and the three existing upper-sided MCV charts 54

Table 3.10 Real bivariate data on the measurements of two diameters monitored simultaneously 57

Table 4.1 LCL, UCL and ARL$_1$ values of the lower-sided and upper-sided Shewhart-MCV charts without measurement error for $p \in \{2, 3\}$ and m = 1 67

Table 4.2 ARL$_0$ values of the lower-sided and upper-sided Shewhart-MCV charts in the presence of measurement errors for p = 2 70

Table 4.3 ARL$_0$ values of the lower-sided and upper-sided Shewhart-MCV charts in the presence of measurement errors for p = 3 71

Table 4.4 ARL$_1$ values of the lower-sided and upper-sided Shewhart-MCV charts in the presence of measurement errors for p = 2 72

Table 4.5 ARL$_1$ values of the lower-sided and upper-sided Shewhart-MCV charts in the presence of measurement errors for p = 3 73

Table 4.6 LCL and ARL$_1$ values of the lower-sided Shewhart-MCV chart, and UCL and ARL$_1$ values of the upper-sided Shewhart-MCV chart with measurement errors for p = 2 and m = 1 78

Table 4.7 LCL and ARL$_1$ values of the lower-sided Shewhart-MCV chart, and UCL and ARL$_1$ values of the upper-sided Shewhart-MCV chart with measurement errors for p = 2 and m = 5 79

Table 4.8 LCL and ARL$_1$ values of the lower-sided Shewhart-MCV chart, and UCL and ARL$_1$ values of the upper-sided Shewhart-MCV chart with measurement errors for p = 3 and m = 1 80

Table 4.9 LCL and ARL_1 values of the lower-sided Shewhart-MCV chart, and UCL and ARL_1 values of the upper-sided Shewhart-MCV chart with measurement errors for p = 3 and m = 5. 81

Table 5.1 $\text{UCL}_{\text{SH-}\gamma}$ values of the upper-sided Shewhart-MCV chart in the presence of measurement errors for various values of θ^2, n, p, m and γ_0 for B = 1 and ARL_0 = 370.4 101

Table 5.2 ARL_1 values for the upper-sided Shewhart-MCV chart in the presence of measurement errors for γ_0 = 0.1 (left), 0.2 (middle) and 0.3 (right), for various values of θ^2, n, p and τ when B = 1, m = 1 and ARL_0 = 370.4 103

Table 5.3 ARL_1 values for the upper-sided Shewhart-MCV chart in the presence of measurement errors for γ_0 = 0.1 (left), 0.2 (middle) and 0.3 (right), for various values of θ^2, n, p and τ when B = 1, m = 3 and ARL_0 = 370.4 104

Table 5.4 ARL_1 values for the upper-sided Shewhart-MCV chart in the presence of measurement errors for γ_0 = 0.1 (left), 0.2 (middle) and 0.3 (right), for various values of θ^2, n, p and τ when B = 1, m = 5 and ARL_0 = 370.4 105

Table 5.5 EARL_1 values for the upper-sided Shewhart-MCV chart in the presence of measurement errors for various values of θ^2, p, n, m and γ_0 when (τ_{min}, τ_{max}) = (1, 2), B = 1 and ARL_0 = 370.4 106

Table 5.6 $\text{UCL}_{\text{SH-}\gamma}$ values of the upper-sided Shewhart-MCV chart in the presence of measurement errors for various values of θ^2, p, n and γ_0 for m = 1, B = 5 and ARL_0 = 370.4...107

Table 5.7 ARL_1 values for the upper-sided Shewhart-MCV chart in the presence of measurement errors for γ_0 = 0.1 (left), 0.2 (middle) and 0.3 (right), for various values of θ^2, n, p and τ when m = 1, B = 5 and ARL_0 = 370.4 109

Table 5.8 EARL_1 values for the upper-sided Shewhart-MCV chart in the presence of measurement errors for various values of θ^2, p, n and γ_0 when (τ_{min}, τ_{max}) = (1, 2), m = 1, B = 5 and ARL_0 = 370.4 ...110

Table 5.9 Values of $\left(\mu_0(\hat{\gamma}^{*2}),\ \sigma_0(\hat{\gamma}^{*2})\right)$ computed in the presence of measurement errors for various values of θ^2, p, n, B and γ_0 when m = 1 and ARL_0 = 370.4 113

Table 5.10 Optimal parameters (λ^*, K^*) and corresponding ARL_1 values of the upper-sided EWMA-γ^2 chart in the presence of measurement errors for various values of θ^2, n, B, γ_0 and τ when m = 1 and p = 2 114

Table 5.11 Optimal parameters (λ^*, K^*) and corresponding ARL_1 values of the upper-sided EWMA-γ^2 chart in the presence of measurement errors for various values of θ^2, n, B, γ_0 and τ when m = 1 and p = 3 115

Table 5.12 Optimal parameters (λ^*, K^*) and corresponding ARL_1 values of the upper-sided EWMA-γ^2 chart in the presence of measurement errors for various values of θ^2, n, B, γ_0 and τ when m = 1 and p = 4 116

Table 5.13 Optimal parameters (λ^*, K^*) and corresponding EARL_1 values of the upper-sided EWMA-γ^2 chart in the presence of measurement errors for various values of θ^2, p, n, B and γ_0 when (τ_{min}, τ_{max}) = (1, 2) and m = 1 118

Table 5.14 Values of $\left(\mu_0(\hat{\gamma}^{*2}),\ \sigma_0(\hat{\gamma}^{*2})\right)$ computed in the presence of measurement errors for various values of θ^2, p, n, m and γ_0 when B = 1 and ARL_0 = 370.4 119

Table 5.15 Optimal parameters (λ^*, K^*) and corresponding ARL_1 values of the upper-sided EWMA-γ^2 chart in the presence of measurement errors for various values of θ^2, n, m, γ_0 and τ when B = 1 and p = 2 120

Table 5.16 Optimal parameters (λ^*, K^*) and corresponding ARL_1 values of the upper-sided EWMA-γ^2 chart in the presence of measurement errors for various values of θ^2, n, m, γ_0 and τ when B = 1 and p = 3 121

Table 5.17 Optimal parameters (λ^*, K^*) and corresponding ARL_1 values of the upper-sided EWMA-γ^2 chart in the presence of measurement errors for various values of θ^2, n, m, γ_0 and τ when B = 1 and p = 4 122

Table 5.18 Optimal parameters (λ^*, K^*) and corresponding $EARL_1$ values of the upper-sided EWMA-γ^2 chart in the presence of measurement errors for various values of θ^2, p, n, m and γ_0 when (τ_{min}, τ_{max}) = (1, 2) and B = 1 123

LIST OF FIGURES

		Page
Figure 1.1	An illustrative example of the two-sided Shewhart chart	2
Figure 2.1	A graphical view of the two one-sided Shewhart-MCV charts	23
Figure 2.2	A graphical view of the upper-sided EWMA-γ^2 chart	29
Figure 2.3	A subdivision of the in-control region into s states, each of width ω	30
Figure 3.1	A graphical view of the upper-sided VSI EWMA-γ^2 chart	42
Figure 3.2	Upper-sided VSI EWMA-γ^2 chart for the data in Table 3.10	58
Figure 4.1	ARL_0 (top) and ARL_1 (bottom) plots when measurement errors are present for p = 2	74
Figure 4.2	ARL_0 (top) and ARL_1 (bottom) plots when measurement errors are present for p = 3	75
Figure 4.3	A summary of the effects of ignoring the presence of measurement errors in computing the limits of the lower-sided and upper-sided Shewhart-MCV charts when such errors actually exist	76
Figure 4.4	ARL_1 plots when the lower-sided and upper-sided Shewhart-MCV charts' limits are specially designed by taking into account of the presence of measurement errors, for p = 2 (top) and p = 3 (bottom) when $m \in \{1, 5\}$	82
Figure 4.5	Shewhart-MCV charts for the Phase-II samples without measurement error when the limits of the charts are computed by assuming that there is no measurement error	85
Figure 4.6	Shewhart-MCV charts for the Phase-II samples with measurement errors when the limits of the charts are computed by assuming that there is no measurement error	85

Figure 4.7 Shewhart-MCV charts for the Phase-II samples with measurement errors when the limits of the charts are computed by assuming that measurement errors exist....86

Figure 4.8 A summary of the findings of the illustrative example....90

Figure 5.1 Upper-sided Shewhart-MCV chart for the Phase-II data in the presence of measurement errors when $\tau = 1$....125

Figure 5.2 Upper-sided EWMA-γ^2 chart for the Phase-II data in the presence of measurement errors when $\tau = 1$....126

Figure 5.3 Upper-sided Shewhart-MCV chart for the Phase-II data in the presence of measurement errors when $\tau = 2$....126

Figure 5.4 Upper-sided EWMA-γ^2 chart for the Phase-II data in the presence of measurement errors when $\tau = 2$....127

LIST OF ABBREVIATIONS

ARL	Average run length
ARL_0	In-control ARL
ARL_1	Out-of-control ARL
ATS	Average time to signal
ATS_0	In-control ATS
ATS_1	Out-of-control ATS
CDF	Cumulative distribution function
CL	Central line
CUSUM	Cumulative sum
CV	Coefficient of variation
EARL	Expected ARL
$EARL_0$	In-control EARL
$EARL_1$	Out-of-control EARL
EATS	Expected ATS
$EATS_0$	In-control EATS
$EATS_1$	Out-of-control EATS
EWMA	Exponentially weighted moving average
LCL	Lower control limit
MCV	Multivariate coefficient of variation
MVN	Multivariate normal
PDF	Probability density function
RR	Run rule
RS	Run sum

SAS	Statistical Analysis System
SDRL	Standard deviation of the run length
SDTS	Standard deviation of the time to signal
$SDTS_0$	In-control SDTS
$SDTS_1$	Out-of-control SDTS
SPC	Statistical Process Control
Syn	Synthetic
UCL	Upper control limit
VSI	Variable sampling interval
VSS	Variable sample size
VSSI	Variable sample size and sampling interval
VP	Variable parameter

LIST OF NOTATIONS

n	Sample size
p	Number of quality characteristics monitored simultaneously
γ	Population MCV
γ^*	Population MCV in the presence of measurement errors
$\hat{\gamma}$	Sample MCV
$\hat{\gamma}^2$	Sample MCV-squared
$\hat{\gamma}^*$	Sample MCV in the presence of measurement errors
γ_0	In-control MCV
γ_1	Out-of-control MCV
$\boldsymbol{\mu}$	Population mean vector
$\boldsymbol{\mu}_0$	In-control population mean vector
$\boldsymbol{\mu}_1$	Out-of-control population mean vector
$\boldsymbol{X}$	Observed vector of quality characteristics
$\boldsymbol{X}^*$	Observed vector of quality characteristics in the presence of measurement errors
$\overline{\boldsymbol{X}}_{ij}^*$	Average of $\boldsymbol{X}_{ij1}^*$, $\boldsymbol{X}_{ij2}^*$, …, $\boldsymbol{X}_{ijm}^*$, for the j-th item of the i-th sample in the presence of measurement errors
$\overline{\overline{\boldsymbol{X}}}_i^*$	Average of $\overline{\boldsymbol{X}}_{i1}^*$, $\overline{\boldsymbol{X}}_{i2}^*$, …, $\overline{\boldsymbol{X}}_{in}^*$, for the i-th sample in the presence of measurement errors
A	Intercept of the linearly covariate error model
B	Slope of the linearly covariate error model
$\boldsymbol{A}$	Vector of constants
$\boldsymbol{B}$	Diagonal matrix of constants
$\boldsymbol{\Sigma}$	Population covariance matrix

$\boldsymbol{\Sigma}_0$	In-control population covariance matrix
$\boldsymbol{\Sigma}_1$	Out-of-control population covariance matrix
$\boldsymbol{S}$	Sample covariance matrix
$\boldsymbol{S}_i^*$	Sample i-th covariance matrix in the presence of measurement errors
$F_{F'}$	Singly non-central F distribution
$F_{F''}$	Doubly non-central F distribution
$F_{F''}^{-1}$	Inverse CDF of the singly non-central F distribution
δ	Non-centrality parameter
δ^*	Non-centrality parameter in the presence of measurement errors
τ	Shift size
τ_{min}	Minimum shift size
τ_{max}	Maximum shift size
(τ_{min}, τ_{max})	Shift size interval
C	Continued fraction
$\mu_1'(F'')$	First raw moment of F''
$\mu_2'(F'')$	Second raw moment of F''
$\tilde{\mu}_1'(F'')$	First trimmed raw moment of F''
$\tilde{\mu}_2'(F'')$	Second trimmed raw moment of F''
$\mu_0(\hat{\gamma}^2)$	In-control mean of $\hat{\gamma}^2$
$\sigma_0(\hat{\gamma}^2)$	In-control standard deviation of $\hat{\gamma}^2$
$f_{F''}$	PDF of F''
ξ	A very small value (i.e. 10^{-4}, 10^{-5}, etc.)
Z_i	EWMA statistic of the i-th sample
h_1	Short sampling interval
h_2	Long sampling interval

H_j	Midpoint of the j-th subinterval
$\boldsymbol{I}$	Identity matrix
$\mathbf{1}$	Vector with all elements equal to unity
λ	Smoothing parameter
α_0	Fixed Type-I error rate
$\boldsymbol{q}$	Vector of initial probabilities
$\boldsymbol{Q}$	Transition probability matrix
$\boldsymbol{g}$	Vector of sampling intervals
ω	Width of the subinterval for the in-control region
$\boldsymbol{\varepsilon}$	Random error term
$\boldsymbol{\Sigma}_{\boldsymbol{\varepsilon}}$	Covariance matrix of $\boldsymbol{\varepsilon}$
m	Number of measurements taken per item
θ^2	Measurement error ratio
$\boldsymbol{\theta}$	Diagonal matrix with all entries θ^2

LIST OF APPENDICES

Appendix A	Optimization programs for the upper-sided VSI EWMA-γ^2 chart and the three competing upper-sided MCV charts
Appendix B	A MATLAB program for the two one-sided Shewhart-MCV charts by ignoring the presence of measurement errors
Appendix C	A MATLAB program for the upper-sided Shewhart-MCV chart in the presence of measurement errors
Appendix D	A MATLAB optimization program for the upper-sided EWMA-γ^2 chart in the presence of measurement errors
Appendix E	Monte Carlo simulation programs in SAS

PELANJUTAN CARTA-CARTA KAWALAN PEKALI VARIASI MULTIVARIAT

ABSTRAK

Carta-carta kawalan untuk mengawal pekali variasi multivariat (MCV) digunakan apabila fokus adalah dalam pemantauan varians multivariat relatif kepada vektor min untuk suatu proses multivariat. Tesis ini mencadangkan carta sisi-atas purata bergerak berpemberat eksponen (EWMA) dengan selang pensampelan boleh berubah (VSI) untuk mengesan anjakan menaik dalam MCV kuasa dua (γ^2), iaitu carta sisi-atas VSI EWMA-γ^2. Formula untuk mengira had-had kawalan dan pengukuran prestasi (menggunakan pendekatan rantaian Markov) carta sisi-atas VSI EWMA-γ^2 telah diberikan. Dapatan kajian menunjukkan bahawa saiz sampel (n) yang besar, bilangan pembolehubah rawak dipantau secara serentak (p) yang kecil dan nilai MCV dalam kawalan (γ_0) yang kecil memberikan pengesanan anjakan proses yang lebih cepat. Kajian perbandingan menunjukkan bahawa carta sisi-atas VSI EWMA-γ^2 mengungguli carta sisi-atas MCV sedia ada untuk pengesanan anjakan menaik dalam MCV proses. Tambahan pula, kesan ralat pengukuran ke atas prestasi carta Shewhart-MCV telah dikaji. Sehubungan itu, tesis ini juga mencadangkan dua carta satu-sisi Shewhart-MCV dengan kehadiran ralat pengukuran untuk mengesan anjakan MCV menurun dan menaik secara berasingan. Sifat-sifat taburan untuk populasi dan sampel MCV dengan model ralat kovariat linear telah diterbitkan. Formula untuk mengira had-had kawalan dan purata panjang larian (ARL) untuk carta-carta Shewhart-MCV berasaskan ralat pengukuran diterbitkan. Suatu prosedur langkah demi langkah yang menjelaskan kesan andaian palsu ketiadaan ralat pengukuran ke atas carta Shewhart-MCV juga diperincikan. Dapatan kajian menunjukkan bahawa untuk carta sisi-bawah

Shewhart-MCV, nilai ARL menjadi lebih besar daripada yang dijangkakan apabila nilai unsur pepenjuru $\boldsymbol{\theta}$ bertambah. Sebaliknya, untuk carta sisi-atas Shewhart-MCV, nilai ARL menjadi lebih kecil daripada yang dijangkakan apabila nilai unsur pepenjuru $\boldsymbol{\theta}$ meningkat. Justeru, carta sisi-bawah dan sisi-atas Shewhart-MCV tidak boleh lagi dipercayai apabila had-had kawalan yang digunakan dikira dengan mengabaikan kehadiran ralat pengukuran walhal pada kenyataanya, ralat pengukuran wujud. Tambahan pula, dalam tesis ini, carta-carta sisi-atas Shewhart-MCV dan EWMA-γ^2 dalam kehadiran ralat pengukuran telah dibangunkan. Suatu pendekatan yang berbeza dalam penerbitan formula populasi dan sampel MCV dengan model ralat kovariat linear digunakan untuk membangunkan kedua-dua carta satu-sisi Shewhart-MCV dan carta satu-sisi Shewhart-MCV. Formula untuk mengira had-had kawalan dan pengukuran prestasi carta-carta sisi-atas Shewhart-MCV dan EWMA-γ^2 dalam kehadiran ralat pengukuran telah diperoleh. Kesan kehadiran ralat pengukuran ke atas kedua-dua carta terkemudian ini telah dikaji. Dapatan kajian menunjukkan bahawa lebih kecil nilai nisbah ralat pengukuran (θ^2), maka lebih cepat carta Shewhart-MCV dan EWMA-γ^2 dalam pengesanan keadaan luar kawalan, yakni, mencerminkan kesan negatif ralat pengukuran ke atas prestasi kedua-dua carta tersebut. Tambahan pula, dengan meningkatkan bilangan kali suatu barang diukur (m) dan nilai unsur pepenjuru matriks $\boldsymbol{B}$, kesan kehadiran ralat pengukuran dapat dikurangkan. Perisian MATLAB digunakan untuk menjalankan semua analisis berangka manakala simulasi dengan perisian SAS digunakan untuk mengesahkan ketepatan pengiraan berangka yang diperoleh dengan menggunakan MATLAB. Akhir sekali, contoh-contoh yang menggunakan data sebenar dibentangkan untuk semua carta yang telah dicadangkan.

EXTENSIONS OF MULTIVARIATE COEFFICIENT OF VARIATION CONTROL CHARTS

ABSTRACT

Control charts for monitoring multivariate coefficient of variation (MCV) are applied when the interest is in monitoring the relative multivariate variability to the mean vector of a multivariate process. This thesis proposes an upper-sided variable sampling interval (VSI) exponentially weighted moving average (EWMA) chart to detect upward shifts in the MCV squared (γ^2), that is, the upper-sided VSI EWMA-γ^2 chart. Formulae to compute the control limits and performance measures (using the Markov chain approach) of the upper-sided VSI EWMA-γ^2 chart are given. The findings show that a large sample size (n), a small number of variables monitored simultaneously (p) and a small value of in-control MCV (γ_0) result in a faster detection of process shifts. Comparative studies show that the upper-sided VSI EWMA-γ^2 chart outperforms the existing upper-sided MCV charts in detecting upward shifts in the process MCV. In addition, the effects of measurement errors on the performances of the Shewhart-MCV chart are studied. Consequently, this thesis also proposes two one-sided Shewhart-MCV charts in the presence of measurement errors for detecting downward and upward MCV shifts separately. The distributional properties of the population and sample MCVs with a linearly covariate error model are derived. The formulae to compute the control limits and average run lengths (ARLs) of these measurement errors based Shewhart-MCV charts are derived. A step-by-step procedure explaining the effects of a false assumption of no measurement error on the Shewhart-MCV charts is detailed. The findings show that for the lower-sided

Shewhart-MCV chart, the ARL value becomes larger than expected as the value of the diagonal elements of $\boldsymbol{\theta}$ increases. On the contrary, for the upper-sided Shewhart-MCV chart, the ARL value becomes smaller than expected as the value of the diagonal elements of $\boldsymbol{\theta}$ increases. Thus, the lower-sided and upper-sided Shewhart-MCV charts are no longer reliable when the control limits adopted are computed by ignoring the presence of measurement errors when in actuality measurement errors exist. Furthermore, in this thesis, the upper-sided Shewhart-MCV and EWMA-γ^2 charts in the presence of measurement errors are developed. A different approach in the formulae derivation of the population and sample MCVs with a linearly covariate error model is used in developing the two one-sided Shewhart-MCV charts and the upper-sided Shewhart-MCV chart. The formulae for computing the control limits and performance measures of the upper-sided Shewhart-MCV and EWMA-γ^2 charts in the presence of measurement errors are derived. The effect of the presence of measurement errors on these two latter charts is studied. The findings show that the smaller the value of the measurement error ratio (θ^2), the faster are the Shewhart-MCV and EWMA-γ^2 charts in detecting an out-of-control situation, indicating the negative effect of measurement errors on the performances on both charts. In addition, by increasing the number of times an item is measured (m) and the value of the diagonal elements of matrix $\boldsymbol{B}$, the effect of the presence of measurement errors is reduced. The MATLAB software is used to conduct all the numerical analyses, while simulation using the SAS software is employed to verify the accuracy of the numerical computations obtained using MATLAB. Finally, illustrative examples using real life data are presented for all the proposed charts.

CHAPTER 1

INTRODUCTION

1.1 Statistical Process Control

Statistical Process Control (SPC) is a powerful statistical technique developed in the 1920s. It is an efficient methodology for controlling the process stability and measuring the quality of a manufacturing process. SPC is an important evaluation tool because it is based on easy to follow principles and can be used in any manufacturing process (Montgomery, 2019).

SPC involves seven graphical tools, which are called "the magnificent seven", namely, stem-and-leaf or histogram, check sheet, Pareto chart, cause-and-effect diagram, defect concentration diagram, scatter diagram and control chart (Montgomery, 2019).

Of the seven important tools, the control chart is the focus of this thesis. The first control chart, called the Shewhart chart was developed in the 20th century by Walter A. Shewhart. A standard control chart is based on a certain statistical distribution and often consists of three control limits, i.e. lower control limit (LCL), central line (CL), and upper control limit (UCL). The x-axis of a control chart represents the sample number, whereas the y-axis represents the value of the statistic (for example, the sample mean, $\bar{X}$). If a sample point plotted on a chart falls outside the control limits, the process is considered as out-of-control and corrective actions should be taken to remove the assignable cause(s). Otherwise, the process is in-control. Figure 1.1 shows an illustrative example of the standard Shewhart chart.

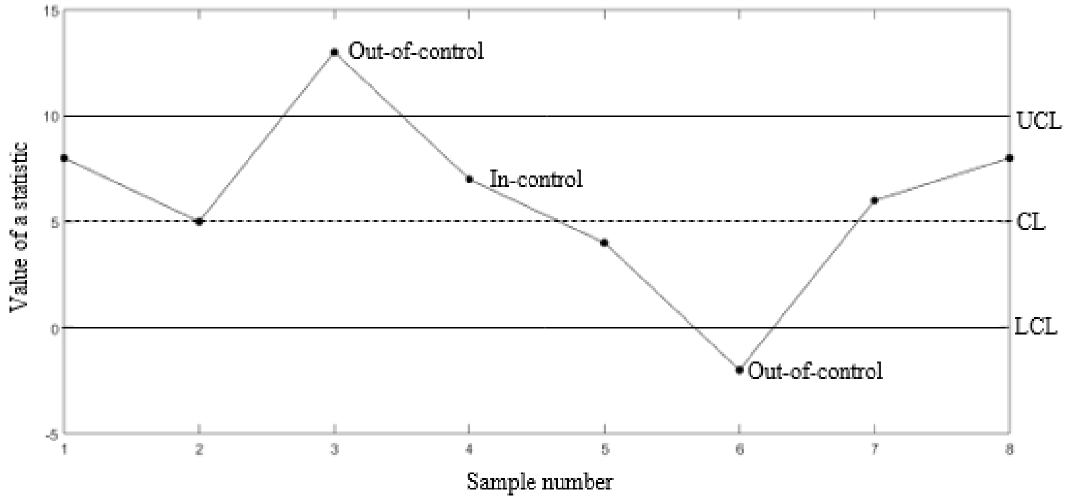

Figure 1.1 An illustrative example of the two-sided Shewhart chart

A two-sided chart detects upward and downward shifts on the same chart, whereas one-sided charts detect either upward or downward shifts. Specifically, upper-sided charts only detect an upward shift, whereas lower-sided charts only detect a downward shift in a process.

The data for a process being monitored are obtained in real-time during manufacturing. The data are plotted on a control chart with pre-determined control limits. In general, the implementation of a control chart must be executed in two phases. Phase-I ensures that the process is suitable for the objectives and confirms what the process should look like. Phase-II monitors the process and makes sure that it continues to perform effectively (Montgomery, 2019).

In Phase-I, a control chart is used to monitor if the process is in statistical control by analyzing the historical dataset. After ensuring that the Phase-I process is in-control, the control limits of the chart can be estimated from the said Phase-I data. In Phase-II, the chart is used to monitor the future data obtained from the same process by comparing the sample statistic for each future sample with the control limits estimated from the Phase-I data. The main purpose of Phase-II is to determine if the process is in statistical control (Woodall, 2000).

The two main types of control charts are control charts for variables and those for attributes. Control charts for variables are used to monitor the variation in the process when the measurement is variable (i.e. it can be measured in terms of continuous values). Examples of variables charts are the $\bar{X}$, R and S charts. Control charts for attributes are used to monitor the variation in the process when the measurements can be taken as a discrete count, for example, the p, np and c charts (Montgomery, 2019).

1.2 Problem Statement

Control charts are usually designed to monitor the mean or variance of a process. However, practitioners may not be interested in the changes in the mean or the variance. They may be interested in monitoring the relative process variability to the process mean, also known as the coefficient of variation (CV) (Kang et al., 2007).

In recent years, control charts for monitoring the CV for a multivariate process has gained growing attention. The standard multivariate coefficient of variation (MCV) chart is used to monitor the relative multivariate variability to the mean vector of a multivariate process. The standard MCV (or Shewhart-MCV) chart is very effective in detecting large shifts in the process MCV. Its disadvantage is that it is relatively insensitive to small shifts (Yeong et al., 2016).

Owing to the skewness of the MCV distribution, the one-sided Shewhart-MCV charts are considered in this thesis. Yeong et al. (2016) mentioned that upward shifts in the process MCV are easier to be detected than downward shifts. Furthermore, detecting upward shifts in the relative multivariate variability to the mean vector in the process MCV is more important as this indicates a large increase in the process variance relative to the process mean (Yeong et al., 2016).

To improve the sensitivity of the Shewhart-MCV chart towards small shifts, Giner-Bosch et al. (2019) proposed an upper-sided exponentially weighted moving average (EWMA) chart for monitoring upward shifts in the process MCV, that is, the EWMA-γ^2 chart. Past research has shown that varying at least one of the charts parameters as a function of prior observations increases the sensitivity of the chart. Therefore, to improve the efficiency of the EWMA-γ^2 chart, the variable sampling interval (VSI) feature is incorporated into the aforesaid chart. Consequently, the new chart's sensitivity in detecting small and moderate shifts increases. Thus, the upper-sided VSI EWMA-γ^2 chart is proposed in this thesis. The VSI EWMA-γ^2 chart is a combination of the VSI technique of Saccucci et al. (1992) and the EWMA-γ^2 chart of Giner-Bosch et al. (2019). The optimization algorithm for the VSI EWMA-γ^2 chart is put forward. The average time to signal (ATS), standard deviation of the time to signal (SDTS) and expected average time to signal (EATS) performances show that the new upper-sided VSI EWMA-γ^2 chart outperforms the existing upper-sided MCV charts.

In real-life experiments, measurement errors occur due to factors which cannot be controlled, such as imprecise measurement devise or human errors. Such errors have significant impact on the process which deteriorate the performance of the chart. There is only very little research that deals with multivariate charts in the presence of measurement errors exists in the literature. To fill this gap, a new Shewhart-MCV chart employing the linearly covariate error model presented in Linna et al. (2001) is developed. The effect of a false assumption of no measurement error on the proposed two one-sided Shewhart-MCV charts when measurement errors actually exist is studied in this thesis. The effect of the presence of measurement errors using different derivation methods on the upper-sided Shewhart-MCV and EWMA-γ^2 charts is also studied.

1.3 Objectives of the Study

The objectives of this study are as follows:

(i) To propose the upper-sided VSI EWMA-γ^2 chart.

(ii) To investigate the effects of a false assumption of no measurement error on the two one-sided Shewhart-MCV charts.

(iii) To propose the two one-sided Shewhart-MCV charts in the presence of measurement errors.

(iv) To develop the upper-sided Shewhart-MCV and EWMA-γ^2 charts in the presence of measurement errors using different derivation methods.

The Shewhart-MCV and EWMA-γ^2 charts are used when researchers are not interested in monitoring the mean vector or covariance matrix of a multivariate process, instead they are interested in monitoring the relative multivariate variability to the mean vector. All the above objectives are enhancements to the Shewhart-MCV chart proposed by Yeong et al. (2016) and EWMA-γ^2 chart developed by Giner-Bosch et al. (2019).

1.4 Significance of the Study

This study aims to increase the sensitivity of existing MCV charts in detecting process shifts by incorporating the VSI scheme into the upper-sided EWMA-γ^2 chart proposed by Giner-Bosch et al. (2019). Besides that, this study investigates the effect of designing the two one-sided Shewhart-MCV charts by ignoring the presence of measurement errors in computing the control limits when in fact such errors exist. Moreover, this study demonstrates the negative effect of measurement errors on the upper-sided Shewhart-MCV and EWMA-γ^2 charts when the control limits of the charts are specially designed for such errors. The effect of multiple times an item is measured is also investigated. The proposed Shewhart-MCV and EWMA-γ^2 charts with measurement errors are recommended for use because when there is no measurement error, researchers can set the level of measurement error as zero.

Researchers will be able to compute the control limits and study the performances of the proposed charts. Researchers will also be able to implement the proposed charts, as step-by-step procedures are explained clearly.

1.5 Limitations of the Study

In this study, the sample size (n) that is larger than the number of variables monitored simultaneously (p) is considered. In the future, problems involving high-dimensional cases, where p is of the same order or larger than n, should be addressed by using other methods, such as regularized or shrinkage estimates that reduces the dimension of the process monitored. Moreover, the analyses in this thesis assume that the underlying process is normally distributed. In order to cater for a nonnormal underlying process, a nonparametric approach can be developed in the future, for monitoring the process MCV.

1.6 Organization of the Thesis

Chapter 1 begins with a summary of SPC, followed by the problem statement and objectives of the thesis. Chapter 2 presents a literature review of the existing CV and MCV charts and an overview of the univariate and multivariate charts with measurement errors. The properties of the two one-sided Shewhart-MCV charts and the upper-sided EWMA-γ^2 chart, along with their performance measures, are described. The linearly covariate error model is also introduced in this chapter.

Chapter 3 discusses the proposed upper-sided VSI EWMA-γ^2 chart, together with the performance measures and optimal design of the chart. The proposed chart is then compared with the existing upper-sided MCV charts, such as the Shewhart-MCV, variable parameters (VP) MCV, and EWMA-γ^2 charts. An illustrative example is given to show the implementation of the proposed VSI EWMA-γ^2 chart in real life.

Chapter 4 proposes the two one-sided Shewhart-MCV charts which consider measurement errors. The effects of a false assumption of no measurement error on the two one-sided Shewhart-MCV charts are studied. The performances of the proposed charts with and without measurement errors are studied. An illustrative example is provided.

Chapter 5 puts forward the upper-sided Shewhart-MCV and EWMA-γ^2 charts in the presence of measurement errors. The formulae for computing the control limits and performance measures of the charts in the presence of measurement errors are derived. Finally, illustrative examples for the proposed charts are provided.

Chapter 6 summarizes the contributions and findings in the thesis. Future research topics are also identified in this chapter.

The programs written in the MATLAB software and Statistical Analysis System (SAS) are presented in Appendices A, B, C, D and E. In Appendix A, MATLAB programs for computing the optimal parameters and ARL using the Markov chain approach for the upper-sided VSI EWMA-γ^2 chart and the three comparative upper-sided MCV charts, namely, the Shewhart-MCV, VP MCV and EWMA-γ^2 charts are provided. A MATLAB program for the performance evaluation of the two one-sided Shewhart-MCV charts by ignoring the presence of measurement errors is given in Appendix B. The MATLAB codes for computing the performance measures of the upper-sided Shewhart-MCV chart in the presence of measurement errors are presented in Appendix C. The MATLAB program incorporating the Markov chain approach to obtain the ARL and the optimal parameters of the upper-sided EWMA-γ^2 chart in the presence of measurement errors are shown in Appendix D. The Monte Carlo simulation programs for all the proposed charts are presented in Appendix E.

CHAPTER 2

A REVIEW OF RELATED CHARTS AND THEIR PERFORMANCE MEASURES

2.1 Introduction

Most of the existing charts focus on monitoring the mean or variance of the quality characteristic of interest (Yeong et al. (2016). In processes when the mean and variance are not constant, that is, the variance is a function of the mean, traditional charts, such as $\bar{X}$, R and S charts are not useful. In such a case, monitoring the sample CV for a univariate process is preferable. The CV chart is used when the process standard deviation is proportional to the process mean. A univariate chart is used for monitoring one variable, whereas a multivariate chart is used for monitoring a multivariate process. In this thesis, the interest is in improving the performance of existing MCV charts in monitoring the relative process variability to the mean vector of a multivariate process. The effects of the presence of measurement errors on different types of MCV charts are also studied.

This chapter is structured as follows: Section 2.2 gives an overview of the univariate and multivariate CV charts. Section 2.3 gives an overview of the univariate and multivariate charts in the presence of measurement errors. Section 2.4 gives the basic definitions and assumptions of the sample MCV. Section 2.5 presents the control limits and performance measures for two types of MCV charts, namely, Shewhart-MCV and EWMA-γ^2 charts. Finally, Section 2.6 briefly reviews the linearly covariate error model.

2.2 Literature Review of the Univariate and Multivariate CV Charts

This section is divided into two subsections. Section 2.2.1 reviews previous studies on the CV charts and Section 2.2.2 presents previous works on the MCV charts.

2.2.1 An overview of CV charts

Many definitions are given for the distribution of the CV, including those by Hendricks and Robey (1936), Iglewicz (1967) and Verrill (2003). The first univariate Shewhart-CV chart was proposed by Kang et al. (2007), where neither the mean nor the variance in the process is constant, but the CV is. The formula to compute the ARL is derived. The two-sided EWMA chart for monitoring the CV was introduced by Hong et al. (2008), who derived formulae to compute the ARL and standard deviation of the run length (SDRL). Subsequently, Castagliola et al. (2011) investigated the two one-sided EWMA charts for monitoring the CV squared, instead of the CV itself. The formulae to compute the ARL and SDRL were derived for known shift sizes, whereas the expected ARL (EARL) was derived for unknown shift sizes.

Calzada and Scariano (2013) developed an upper-sided synthetic (Syn) chart for monitoring the CV and called it Syn-CV. The comparative studies show that the Syn-CV chart outperforms the Shewhart-CV chart proposed by Kang et al. (2007) and the EWMA CV-squared chart proposed by Castagliola et al. (2011) for large upward shifts in the process CV. For small upward shifts, the EWMA CV-squared chart outperforms the Syn-CV chart. Castagliola et al. (2013a) presented a new efficient method for monitoring the CV chart using run rules (RR). Castagliola et al. (2013b) investigated the CV chart using the VSI scheme. They derived formulae of the performance measures for known shift sizes, in terms of the ATS and SDTS criteria, and for unknown shift sizes, in terms of the EATS criterion. The comparison shows that the VSI CV chart outperforms the Shewhart-CV chart. Thereafter, Zhang et al. (2014) proposed a modified EWMA chart to monitor the CV.

Castagliola et al. (2015a) presented the CV chart using the variable sample size (VSS) scheme. They derived the performance measures in terms of ARL, SDRL, average sample size (ASS) and EARL. The comparative results revealed that the VSS CV chart outperforms the Shewhart-CV, VSI CV and Syn-CV charts. Castagliola et al. (2015b) considered a new method to monitor two one-sided CV charts in a short production runs environment. They derived formulae to compute the performance measures of the proposed charts, in terms of truncated average run length (TARL) and truncated standard deviation of the run length (TSDRL). You et al. (2016) proposed a side-sensitive group runs chart for monitoring the CV. Khaw et al. (2017) studied the CV chart using the variable sample size and sampling interval (VSSI) scheme. The formulae of the performance measures are derived using the Markov chain approach. The comparative studies showed that the VSSI CV chart outperforms all existing CV charts, such as the VSI CV, VSS CV, EWMA CV-squared, Syn-CV, RR CV and Shewhart-CV charts, except the EWMA CV-squared chart when the shift is very small.

Yeong et al. (2017b) proposed a direct procedure to monitor the CV using the VSS scheme. Yeong et al. (2017c) presented the upper-sided VSI EWMA chart for monitoring the CV squared, and they derived formulae for the performance measures, in terms of the ATS, SDTS and EATS criteria using the Markov chain approach. The comparative studies showed that the chart proposed by Yeong et al. (2017c) outperforms the upper-sided Shewhart-CV chart proposed by Kang et al. (2007), Syn CV chart proposed by Calzada and Scariano (2013), and EWMA CV-squared chart proposed by Castagliola et al. (2011). Muhammad et al. (2018) developed the VSS

EWMA chart for monitoring the CV squared, and they derived formulae for computing the ARL, SDRL, ASS and EARL values. The results showed that the VSS EWMA CV-squared chart outperforms the existing CV charts.

Later, Yeong et al. (2018) suggested the CV chart using the VP scheme and they derived formulae to compute the ATS and SDTS values. The results showed that the VP CV chart outperforms the VSI CV, VSS CV, VSSI CV, EWMA CV-squared, Syn-CV and Shewhart-CV charts for large and moderate CV shifts but the EWMA CV-squared outperforms the VP CV chart for small CV shifts. Noor-ul-Amin and Riaz (2020) proposed the EWMA chart for monitoring the CV using log-normal transformation based on ranked set sampling. Finally, Yeong et al. (2021) presented the side-sensitive Syn CV chart. The comparative studies show that the side-sensitive Syn CV chart outperforms the existing Shewhart-CV and Syn-CV charts.

2.2.2 An overview of MCV charts

Many definitions for the MCV are available, such as those by Voinov and Nikulin (1996), Albert and Zhang (2010), and Aerts et al. (2015). The first multivariate chart for monitoring the MCV was the two one-sided Shewhart-type MCV charts proposed by Yeong et al. (2016). The two one-sided Shewhart-MCV charts are the upper-sided and lower-sided Shewhart-MCV charts used to monitor upward and downward shifts in the MCV, respectively. Like any Shewhart-type charts, the chart proposed by Yeong et al. (2016) for monitoring the MCV is sensitive to large shifts but insensitive to moderate and small shifts. To improve the performance of the Shewhart-MCV chart proposed by Yeong et al. (2016), Lim et al. (2017) proposed two one-sided run sum (RS) charts for monitoring the process MCV. The chart proposed by Lim et al.

(2017) showed that the RS technique effectively enhances the detection ability of the Shewhart-MCV chart proposed by Yeong et al. (2016).

Abbasi and Adegoke (2018) studied the MCV chart in Phase-I of SPC because previous works on monitoring the MCV have been done in Phase-II. Abbasi and Adegoke (2018) demonstrated the importance of Phase-I procedure, which reflect real-life situation and are dependent on the historical samples. Phase-I procedure involves the estimation of the control limits from a historical dataset that comes from the in-control process (i.e. if the in-control parameters are unknown, the dataset from Phase-I is used to estimate the control limits).

To improve the sensitivity of the Shewhart-MCV chart in detecting small and moderate shifts, Khaw et al. (2018) proposed three adaptive schemes for monitoring the process MCV. The three adaptive schemes are the VSI, VSS and VSSI schemes. Khaw et al. (2018) designed the aforementioned charts using the Markov chain approach and they compared the performances of their charts with the Shewhart-MCV chart proposed by Yeong et al. (2016) for known shift sizes, in terms of the ATS and SDTS criteria and for unknown shift sizes, in terms of the EATS criterion. The performance comparison shows that the VSSI MCV chart outperforms the existing MCV charts. Khaw et al. (2018) showed that by allowing the sample size and sampling interval to vary, researchers can have better control in process monitoring, which allows a quicker detection of an out-of-control signal.

Giner-Bosch et al. (2019) proposed an upper-sided EWMA chart for monitoring upward shifts in the process MCV-squared (γ^2), that is, the EWMA-γ^2 chart. Giner-Bosch et al. (2019) designed their proposed chart using the Markov chain approach, derived formulae to compute the control limits and performance measures, and determined the optimal parameters of the proposed chart. A performance comparison of the upper-sided Shewhart-MCV chart proposed by Yeong et al. (2016), upper-sided RS MCV chart proposed by Lim et al. (2017) and upper-sided EWMA-γ^2 chart proposed by Giner-Bosch et al. (2019) showed that the upper-sided EWMA-γ^2 chart outperforms the other two MCV charts, in terms of ARL and SDRL criteria.

Khaw et al. (2019) proposed an upper-sided Syn chart for monitoring the MCV and they derived formulae and optimization algorithms for investigating the chart's performance. The comparison results of the upper-sided Syn MCV chart with the upper-sided Shewhart-MCV and RS MCV charts proposed by Yeong et al. (2016) and Lim et al. (2017), respectively, indicated that the upper-sided Syn MCV chart outperforms the other two upper-sided MCV charts, in terms of the ARL, SDRL and EARL criteria.

Nguyen et al. (2019a) proposed a VSI Shewhart-type chart for monitoring the MCV. They used time varying sampling intervals, where the sampling interval to take the next sample depends on the location of the previous sample plotted on the chart. This procedure helps the chart to detect process shifts faster. Moreover, Nguyen et al. (2019b) proposed two one-sided Syn charts for monitoring the MCV. They used a Markov chain approach under the zero-state and steady-state conditions to evaluate the performances of the proposed charts. A comparison between the charts proposed by Nguyen et al. (2019b) and the RS MCV chart developed by Lim et al. (2017) showed that the former outperforms the RS MCV chart for detecting upward shifts in the process MCV under the zero-state condition. However, the latter performs better than the former in detecting downward MCV shifts. Finally, Nguyen et al. (2019b) compared the performance of the upper-sided Syn MCV chart with three adaptive upper-sided MCV charts developed by Khaw et al. (2018) under the steady-state condition. The comparison showed that the upper-sided Syn MCV chart performs better than the upper-sided VSI MCV chart in most cases.

Haq and Khoo (2019a) proposed two adaptive EWMA (AEWMA) charts for monitoring the univariate and multivariate CV, that is, the AEWMA CV and the AEWMA MCV charts, respectively. They used the Monte Carlo simulation approach to compute the values of the performance measures. Haq and Khoo (2019a) demonstrated that the AEWMA CV chart performs better than the existing EWMA and cumulative sum (CUSUM) CV charts for detecting large shifts in the process. The AEWMA MCV chart was found to perform better than the Shewhart-MCV chart proposed by Yeong et al. (2016).

Chew et al. (2019) proposed an upper-sided VP chart for monitoring the MCV. They derived formulae and optimization algorithms to obtain the performance measures using the Markov chain approach. The performance comparison in terms of the ATS, SDTS and EATS criteria revealed that the upper-sided VP MCV chart outperforms the upper-sided Shewhart-MCV chart proposed by Yeong et al. (2016), the upper-sided VSSI MCV chart proposed by Khaw et al. (2018) and the upper-sided Syn MCV chart proposed by Khaw et al. (2019).

Khatun et al. (2019) proposed two one-sided charts for monitoring the MCV in short production runs. They derived formulae to compute the performance measures of the proposed MCV charts in terms of TARL, TSDRL and expected truncated average run length (ETARL) criteria. Chew and Khaw (2020) developed a lower-sided chart for monitoring the MCV using the VSSI scheme by means of the Markov chain approach. The lower-sided VSSI MCV chart monitors downward shifts in the process MCV. The results showed that the lower-sided VSSI MCV chart outperforms the existing lower-sided Shewhart, VSI and VSS MCV charts.

Chew et al. (2020a) investigated the efficiency of the RR MCV chart using the Markov chain approach in terms of the ARL and EARL criteria. The results showed that the RR MCV chart surpasses the Shewhart-MCV chart for detecting small and moderate shifts in the process MCV. Thereafter, Chew et al. (2020b) evaluated the performance of the RR MCV chart for short production runs in terms of the TARL and ETARL criteria using the Markov chain approach. The RR MCV chart outperforms the Shewhart-MCV chart in detecting small and moderate MCV shifts in short production runs.

2.3 An Overview of Existing Univariate and Multivariate Charts with Measurement Errors

Many researchers in SPC have studied the effect of measurement errors on univariate charts. Bennett (1954) was the person to study the effects of the linearly covariate error model on the Shewhart-type chart based on $X = Y + \varepsilon$, where X and Y are the observed and true values of the quality characteristic, respectively, and ε is the random error term. Thereafter, Abraham (1977) studied the effects of measurement errors on control charts using the same formula proposed by Bennett (1954). Kanazuka (1986) studied the effects of measurement errors on the power of $\bar{X}$ and R charts. Mittag (1995) studied the performance of the Shewhart chart in the presence of measurement errors. Later, Mittag and Stemann (1998) studied the effects of measurement errors on joint $\bar{X}$ and S charts. Linna and Woodall (2001) proposed a linearly covariate error model for $\bar{X}$ and S^2 charts using a different formula from that proposed by Bennett (1954). Stemann and Weihs (2001) studied the effects of measurement errors on the

EWMA chart for mean and standard deviation using the formula proposed by Bennett (1954). Maravelakis et al. (2004) investigated the effect of measurement errors on the EWMA-type chart using the formula introduced by Linna and Woodall (2001). Costa and Castagliola (2011) studied the joint effect of autocorrelation and measurement errors on the $\bar{X}$ chart. Maravelakis (2012) adopted the model proposed by Linna and Woodall (2001) to study the effects of measurement errors on the CUSUM chart.

More recently, Saghaei et al. (2014) studied the effect of measurement errors on the economic design of the EWMA chart. Haq et al. (2015) studied the EWMA chart in the presence of measurement errors based on ranked set sampling. Hu et al. (2015) investigated the effect of measurement errors on the Syn $\bar{X}$ chart. Dizabadi et al. (2016) explored the effect of measurement errors on the performance of maximum EWMA and mean squared deviation chart with the linearly increasing-type variance. Yeong et al. (2017a) carried out a study on the effect of measurement errors on the univariate CV chart. Nguyen et al. (2019c) proposed the VSI Shewhart chart for monitoring the CV with measurement errors. Tran et al. (2019a) investigated the performances of Shewhart and EWMA charts for monitoring the CV when measurement errors are present. Finally, Tran et al. (2019b) proposed the CUSUM chart for monitoring the CV in the presence of measurement errors.

Only a few researchers have studied the effects of the linearly covariate error model on multivariate charts. The multivariate chart with measurement errors was first proposed by Linna et al. (2001) who analyzed the performance of the fixed sampling rate Hotelling's T^2 chart in the presence of measurement errors. They used the following formula: $\boldsymbol{X} = \boldsymbol{A} + \boldsymbol{BY} + \boldsymbol{\varepsilon}$, where $\boldsymbol{A}$ is a $p \times 1$ vector of constants, $\boldsymbol{B}$ is a $p \times p$ diagonal matrix of constants, $\boldsymbol{Y}$ is a $p \times 1$ vector of quality characteristics, $\boldsymbol{X}$ is a $p \times$

1 vector of observed values and $\boldsymbol{\varepsilon}$ is a $p \times 1$ random vector (assumed to be independent of $\boldsymbol{Y}$) which follows a multivariate normal distribution with a mean vector of zeros and covariance matrix $\boldsymbol{\Sigma}$, denoted as $\boldsymbol{\varepsilon} \sim \text{MVN}(\mathbf{0}, \boldsymbol{\Sigma})$. Chattinnawat and Bilen (2017) studied the effects of multivariate inspection errors on the performance of Hotelling's T^2 chart for multivariate individual observations. Amiri et al. (2018) investigated the effect of measurement errors in a joint monitoring of the mean vector and covariance matrix of a multivariate process using a multivariate chart. Sabahno et al. (2018) analyzed the effect of the presence of measurement errors on the VSI Hotelling's T^2 charts. Sabahno et al. (2019) also investigated the performance of the VSS Hotelling's T^2 chart with measurement errors. Finally, Sabahno et al. (2020) proposed an adaptive multivariate VP chart for a simultaneous monitoring of the mean vector and covariance matrix in the presence of measurement errors using the Markov chain approach.

2.4 Basic Definitions and Assumptions of the Sample MCV

Suppose that there exist p-dimensional quality characteristics of size n, that is, $\boldsymbol{X}_j$, $j = 1, 2, \ldots, n$, where n is the sample size, from a multivariate normal (MVN) distribution with a nonzero mean vector ($\boldsymbol{\mu}$) and a covariance matrix ($\boldsymbol{\Sigma}$), denoted as $\boldsymbol{X} \sim \text{MVN}(\boldsymbol{\mu}, \boldsymbol{\Sigma})$. The population MCV is defined as follows (Voinov and Nikulin, 1996):

$$\gamma = (\boldsymbol{\mu}^{\mathrm{T}} \boldsymbol{\Sigma}^{-1} \boldsymbol{\mu})^{-\frac{1}{2}}. \tag{2.1}$$

To estimate the sample MCV denoted as $\hat{\gamma}$, $\boldsymbol{\mu}$ and $\boldsymbol{\Sigma}$ in Equation (2.1) are estimated with the sample mean vector ($\overline{\boldsymbol{X}}$) and the sample covariance matrix ($\boldsymbol{S}$), respectively, as

$$\overline{\boldsymbol{X}} = \left(\frac{1}{n}\sum_{j=1}^{n} X_{j1}, \ \ldots, \frac{1}{n}\sum_{j=1}^{n} X_{jp}\right)^{\mathrm{T}} \tag{2.2}$$

and

$$\boldsymbol{S} = \frac{1}{n-1}\sum_{j=1}^{n}(\boldsymbol{X}_j - \overline{\boldsymbol{X}})(\boldsymbol{X}_j - \overline{\boldsymbol{X}})^{\mathrm{T}}. \tag{2.3}$$

Consequently, $\hat{\gamma}$ is computed as

$$\hat{\gamma} = (\overline{\boldsymbol{X}}^{\mathrm{T}}\boldsymbol{S}^{-1}\overline{\boldsymbol{X}})^{-\frac{1}{2}}, \tag{2.4}$$

as mentioned in Yeong et al. (2016).

Yeong et al. (2016) adopted Wijsman (1957) theorem and showed that letting $T^2 = n\overline{\boldsymbol{X}}^{\mathrm{T}}\boldsymbol{S}^{-1}\overline{\boldsymbol{X}}$ gives

$$\frac{T^2}{n-1}.\frac{n-p}{p} \sim F_{F'}(p, n-p, \delta), \tag{2.5}$$

where $F_{F'}(\nu_1, \nu_2, \delta)$ is a singly non-central F distribution with ν_1 and ν_2 degrees of freedom and non-centrality parameter $\delta = n\boldsymbol{\mu}^{\mathrm{T}}\boldsymbol{\Sigma}^{-1}\boldsymbol{\mu}$. In general, this distribution is written as the doubly non-central F distribution, denoted as $F_{F''}(\nu_1, \nu_2, \delta_1, \delta_2)$ with the second non-centrality parameter δ_2 = 0. For more details, see Walck (2007).

Yeong et al. (2016) adopted Wijsman's theorem and derived the distribution of $\hat{\gamma}$. From Equation (2.4), $n\hat{\gamma}^{-2} = n\overline{\boldsymbol{X}}^{\mathrm{T}}\boldsymbol{S}^{-1}\overline{\boldsymbol{X}}$. Consequently, Equation (2.5) gives

$$\frac{n\hat{\gamma}^{-2}}{n-1}.\frac{n-p}{p} = \frac{n(n-p)}{(n-1)p\hat{\gamma}^2} \sim F_{F'}(p, n-p, \delta), \tag{2.6}$$

where $\delta = n\boldsymbol{\mu}^{\mathrm{T}}\boldsymbol{\Sigma}^{-1}\boldsymbol{\mu}$. From Equation (2.1), δ can be written as $\delta = n\gamma^{-2}$.

Using the following equivalence $\left(F_{F''}(\nu_1, \nu_2, \delta_1, \delta_2)\right)^{-1} \equiv F_{F''}(\nu_2, \nu_1, \delta_2, \delta_1)$, and with some algebraic manipulations in Equation (2.6), gives

$$\frac{(n-1)p}{n(n-p)}\hat{\gamma}^2 \sim F_{F''}(n-p, p, 0, \delta). \tag{2.7}$$

Yeong et al. (2016) derived an expression for the cumulative distribution function (CDF) of $\hat{\gamma}$ as follows:

$$
\begin{aligned}
F_{\hat{\gamma}}(u|n,p,\delta) &= P(\hat{\gamma} \le u) \\
&= P\left(\frac{1}{\hat{\gamma}} \ge \frac{1}{u}\right) \\
&= P\left(\frac{n(n-p)}{(n-1)p\hat{\gamma}^2} \ge \frac{n(n-p)}{(n-1)pu^2}\right) \\
&= 1 - F_{F'}\left(\frac{n(n-p)}{(n-1)pu^2}\middle| p, n-p, \delta\right),
\end{aligned} \tag{2.8}
$$

where $F_{F'}(\,.\,|p, n-p, \delta)$ is the singly non-central F distribution function with p and $n-p$ degrees of freedom and non-centrality parameter $\delta = n\gamma^{-2}$.

Yeong et al. (2016) demonstrated that with some manipulations, letting $F_{\hat{\gamma}}^{-1}(\alpha|n,p,\delta) = u$ gives $F_{\hat{\gamma}}(u|n,p,\delta) = \alpha$. Thus, the inverse CDF of $\hat{\gamma}$ can be derived as follows. Equation (2.8) gives

$$
1 - F_{F'}\left(\frac{n(n-p)}{(n-1)pu^2}\middle| p, n-p, \delta\right) = \alpha.
$$

Then

$$
\frac{n(n-p)}{(n-1)pu^2} = F_{F'}^{-1}(1-\alpha|p, n-p, \delta).
$$

It follows that

$$
u = \sqrt{\frac{n(n-p)}{(n-1)p}\left[\frac{1}{F_{F'}^{-1}(1-\alpha|p, n-p, \delta)}\right]}.
$$

As $F_{\hat{\gamma}}^{-1}(\alpha|n,p,\delta) = u$, the following is obtained

$$
F_{\hat{\gamma}}^{-1}(\alpha|n,p,\delta) = \sqrt{\frac{n(n-p)}{(n-1)p}\left[\frac{1}{F_{F'}^{-1}(1-\alpha|p, n-p, \delta)}\right]}, \tag{2.9}
$$

where $F_{F'}^{-1}(\,.\,|p, n-p, \delta)$ is the inverse CDF of the singly non-central F distribution with p and $n-p$ degrees of freedom and non-centrality parameter $\delta = n\gamma^{-2}$.

Moreover, the CDF of the sample MCV-squared, denoted as $\hat{\gamma}^2$, can be derived as follows:

$$\begin{aligned} F_{\hat{\gamma}^2}(u|n,p,\delta) &= P(\hat{\gamma}^2 \le u) \\ &= P\left(\frac{1}{\hat{\gamma}^2} \ge \frac{1}{u}\right) \\ &= P\left(\frac{n(n-p)}{(n-1)p\hat{\gamma}^2} \ge \frac{n(n-p)}{(n-1)pu}\right) \\ &= 1 - F_{F'}\left(\frac{n(n-p)}{(n-1)pu}\middle| p, n-p, \delta\right), \end{aligned} \tag{2.10}$$

where $F_{F'}(\,.\,|p,n-p,\delta)$ is the singly non-central F distribution with p and $n-p$ degrees of freedom and non-centrality parameter $\delta = n\gamma^{-2}$, as discussed in Giner-Bosch et al. (2019).

The MCV chart plots the successive MCV samples. An out-of-control signal is detected when $\hat{\gamma}$, computed using Equation (2.4), deviates from the in-control MCV (i.e. γ_0) and plots beyond the limits of the MCV chart. The Phase-I data are collected in advance to set up the control limits of the MCV chart. For sample i in the Phase-I data, $\bar{\boldsymbol{X}}$ and $\boldsymbol{S}$ can be computed using Equations (2.2) and (2.3), respectively. Furthermore, $\hat{\gamma}$ is computed using Equation (2.4) for sample i (i = 1, 2, …) (Yeong et al., 2016).

Following the suggestion of Yeong et al. (2016), to check whether the process MCV is constant, a similar approach to that in Kang et al. (2007) for the univariate case is adopted. For the multivariate case, by applying a regression analysis on $\hat{\gamma}_i^2$ against $\bar{\boldsymbol{X}}_i^{\mathrm{T}}\bar{\boldsymbol{X}}_i$, for i = 1, 2, ..., w, if no significant relationship between $\hat{\gamma}_i^2$ and $\bar{\boldsymbol{X}}_i^{\mathrm{T}}\bar{\boldsymbol{X}}_i$ is concluded, then the process MCV is assumed to be constant. Here, w is the number of Phase-I samples. Yeong et al. (2016) suggested estimating γ_0 using the root mean square method as follows:

$$\hat{\gamma}_0 = \sqrt{\frac{\sum_{i=1}^{w} \hat{\gamma}_i^2}{w}}. \tag{2.11}$$

2.5 Performance Measures of the MCV Charts

This section is divided into two subsections. Sections 2.5.1 and 2.5.2 present the performance measures of the Shewhart-MCV and EWMA MCV charts, respectively, in terms of the ARL, SDRL and EARL criteria.

2.5.1 Performance measures of the Shewhart-MCV chart

Owing to the skewness of the $\hat{\gamma}$ distribution, Yeong et al. (2016) suggested two one-sided Shewhart-MCV charts for monitoring upward and downward MCV shifts separately. The upper-sided chart that detects the upward MCV shifts is the upper-sided Shewhart-MCV chart. The lower-side chart that detects the downward MCV shifts is the lower-sided Shewhart-MCV chart.

For the lower-sided Shewhart-MCV chart, the LCL is set such that the Type-I error rate is equal to α_0. Thus, the LCL is equal to

$$\mathrm{LCL} = F_{\hat{\gamma}}^{-1}(\alpha_0 | n, p, \delta_0), \tag{2.12}$$

where $\delta_0 = n\gamma_0^{-2}$. When $\hat{\gamma}$ < LCL, the process is considered as out-of-control, and corrective actions should be taken to locate and remove the assignable cause(s).

Similarly, for the upper-sided Shewhart-MCV chart, the UCL is set such that the Type-I error rate is equal to α_0. Thus, the UCL is equal to

$$\mathrm{UCL} = F_{\hat{\gamma}}^{-1}(1 - \alpha_0 | n, p, \delta_0). \tag{2.13}$$

when $\hat{\gamma}$ > UCL, the process is considered as out-of-control, and corrective actions should be taken to locate and remove the assignable cause(s).

Figure 2.1 shows a graphical view of the two one-sided Shewhart-MCV charts. The lower-sided Shewhart-MCV chart is on the left and the upper-sided MCV chart is on the right.

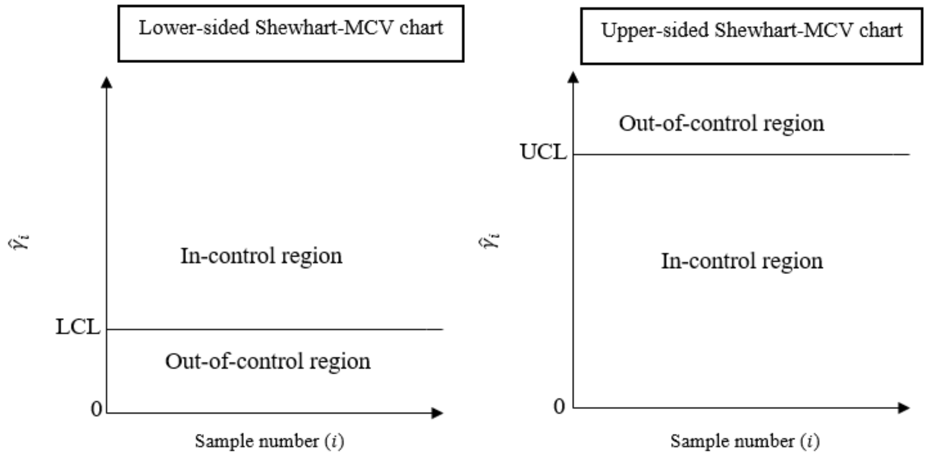

Figure 2.1 A graphical view of the two one-sided Shewhart-MCV charts

The computation of P, i.e. the probability of signalling an out-of-control by the lower-sided and upper-sided Shewhart-MCV charts are given in Equations (2.14) and (2.15), respectively.

$$P = P(\hat{\gamma} < \mathrm{LCL}) = F_{\hat{\gamma}}(\mathrm{LCL}|n, p, \delta_1) \tag{2.14}$$

and

$$P = P(\hat{\gamma} > \mathrm{UCL}) = 1 - F_{\hat{\gamma}}(\mathrm{UCL}|n, p, \delta_1), \tag{2.15}$$

where $\delta_1 = n\gamma_1^{-2}$.

The performance of a control chart can be measured in terms of the ARL criterion, that is, the number of samples that needs to be drawn on the average to obtain a sample statistic plotted beyond the chart's control limits. The ARL_1 and SDRL_1 for the Shewhart-MCV chart can be computed as

$$\mathrm{ARL}_1 = \frac{1}{P} \tag{2.16}$$

and

$$\mathrm{SDRL}_1 = \frac{\sqrt{1-P}}{P}, \tag{2.17}$$

where P is defined in Equations (2.14) and (2.15) for the lower-sided and upper-sided Shewhart-MCV charts, respectively. When the shift size $\tau = 1$, the in-control ARL (ARL_0) and SDRL (SDRL_0) are obtained. When $\tau \neq 1$, the out-of-control ARL (ARL_1) and SDRL (SDRL_1) are obtained. Note that $\tau = \gamma_1/\gamma_0$.

The computation of ARL_1 requires a known shift size (τ). However, when τ is unknown, researchers are often interested in detecting shifts that fall in the interval (τ_{min}, τ_{max}). In this case, the statistical performance of the Shewhart-MCV chart can be computed using the out-of-control EARL (EARL_1) defined as

$$\mathrm{EARL}_1 = \int_{\tau_{min}}^{\tau_{max}} \mathrm{ARL}_1 \times f_\tau(\tau)\, d\tau, \tag{2.18}$$

where τ_{max} is the upper bound of the shift size, τ_{min} is the lower bound of the shift size, $f_\tau(\tau)$ is the probability density function (PDF) of the shift size τ, and ARL_1 is defined in Equation (2.16). The in-control EARL (EARL_0) is set as ARL_0.

The actual shape of $f_\tau(\tau)$ is difficult to determine. Castagliola et al. (2011) suggested a uniform distribution over two different ranges of shifts, i.e. (τ_{min}, τ_{max}) = (1, 2] for monitoring the upward MCV shifts and (τ_{min}, τ_{max}) = [0.5, 1) for monitoring the downward MCV shifts. The Gauss-Legendre quadrature method is used to compute the integration in Equation (2.18). More details on the Gauss-Legendre quadrature method can be found in Kovvali (2011).

2.5.2 Performance measures of the EWMA-γ^2 chart

For the EWMA-γ^2 chart, the MCV-squared (γ^2) is monitored instead of the MCV (γ) itself. Castagliola et al. (2011) showed that monitoring S^2 using the EWMA chart is more efficient than monitoring S using the same chart. As a similar idea to that of Castagliola et al. (2011), monitoring γ^2 instead of γ is also expected to be more efficient for the MCV chart. For more details, see Giner-Bosch et al. (2019).

The EWMA-MCV chart proposed in this thesis is an upper-sided chart (i.e. it detects upward MCV shifts). The detection of upward shifts in the MCV is given more interest because Castagliola et al. (2011) showed that the detection effectiveness of the said shifts the upper-sided CV chart is higher than that of the two-sided CV chart. Giner-Bosch et al. (2019) proposed the upper-sided EWMA-γ^2 chart for monitoring upward shifts in the process MCV, based on the following statistics:

$$Z_i = \lambda \hat{\gamma}_i^2 + (1-\lambda) Z_{i-1}, \tag{2.19}$$

where λ ($\in (0, 1]$) is a smoothing constant to be determined and $\hat{\gamma}_i^2$ is the value of the sample MCV squared at sample i. Notably, the initial value Z_0 is taken as the in-control mean of $\hat{\gamma}^2$, and the approximate form is computed using either Equation (2.24) or (2.28), depending on the value of p.

Giner-Bosch et al. (2019) provided an accurate approximation to compute $\mu_0(\hat{\gamma}^2)$ and $\sigma_0(\hat{\gamma}^2)$ because there is no closed form for the in-control mean and standard deviation of $\hat{\gamma}^2$. They computed the first and second raw moments of the doubly non-central F distribution with $n-p$ and p degrees of freedom and non-centrality parameters 0 and $\delta_0 = n\gamma_0^{-2}$, denoted as $F'' \sim F_{F''}(n-p, p, 0, \delta_0)$.

The expressions used to denote the first and second raw moments of F'' are

$$\mu_1'(F'') = \frac{p}{2}\,\mathrm{C}\left(\frac{p}{2} - 1, -\frac{\delta_0}{2}\right), \tag{2.20}$$

and